



Research Article

# Preparation and characterization of proton exchange polyvinylidene fluoride membranes incorporated with sulfonated mesoporous carbon/SPEEK nanocomposite

Athul Seshadri Ramanujam<sup>1</sup> · Noel Jacob Kaleekkal<sup>2</sup>  · P. Suresh Kumar<sup>1</sup>

Received: 2 September 2019 / Accepted: 10 March 2020 / Published online: 18 March 2020  
© Springer Nature Switzerland AG 2020

## Abstract

Sulfonation of mesoporous carbon CMK-3 (sCMK-3) prepared by nano-casting technique was carried out post synthesis using one-step process. The incorporation of the acid groups was confirmed using XRD, Raman spectroscopy, FTIR, SEM, TEM and BET isotherm. The sCMK-3 was incorporated into sulfonated poly(ether ether ketone) to form a nanocomposite which was introduced into polyvinylidene fluoride matrix to form a proton exchange membrane. The physicochemical characteristics of the nanocomposite incorporated membranes were characterized using FTIR, ionic exchange capacity, water uptake, swelling ratio, mechanical stability and TGA. The nanocomposite incorporated membranes showed greater surface wettability and higher ion-exchange capacity. The presence of the  $-\text{SO}_3\text{H}$  acid groups plays a major role in improving the proton conductivity through the Grotthuss-type mechanism. M4 membrane was identified to be a suitable replacement in the DMFC as it had sufficiently high tensile strength (862.2 MPa), high proton conductivity ( $0.081 \text{ S cm}^{-1}$ ) at  $45^\circ\text{C}$  and ultra-low methanol permeability ( $2.17 \times 10^{-8} \text{ cm}^2 \text{ s}^{-1}$ ). No evident hydrolytic damage could be identified and had sufficiently high thermal stability and hence can be proposed as a suitable alternative for Nafion membranes in high temperature, low humidity DMFC applications.

**Keywords** Mesoporous carbon · Proton exchange membrane · Nanocomposite · Proton conductivity · Methanol permeability

## 1 Introduction

The power requirement is directly proportional to the population growth as well as the industrial demand for any country. Though there are myriad drawbacks, first-generation coal-fired power plants still continue to be the major source of power in India [1]. The negative impact of these natural resources on the environment coupled with their diminishing availability paved the way towards the development of alternate sources of power. The landmark Paris Accord also provided a substantial shift toward cleaner, greener fuels and energy technology. Of

the available technologies, fuel cells are widely explored and is a promising source of alternate energy that can be seamlessly integrated into the current technologies [2].

The fuel cell technology was explored initially by Sir William Grove in 1838 and successfully employed on NASA's Gemini space programme in the 1960s [3]. Since then, a large amount of research has been carried out on improving every component of the fuel cell. Of the various types of fuel cells, proton exchange membrane fuel cells (PEMFCs) are being widely explored as it enables efficient fuel transportation for portable power and is one of the most pollution-free sources of energy [4, 5].

✉ Noel Jacob Kaleekkal, noeljacob89@gmail.com; noel@nitc.ac.in | <sup>1</sup>School of Chemical and Biotechnology, SASTRA Deemed to be University, Tanjore 613401, India. <sup>2</sup>Membrane Separation Group, Department of Chemical Engineering, National Institute of Technology Calicut (NITC), Kozhikode, Kerala 673601, India.



Typically, PEMFC operation involves the oxidation of H<sub>2</sub> fuel at the anode which liberates protons and electrons. The protons are transported across a suitable polymeric membrane to the cathode where they recombine with the electrons and react with supplied O<sub>2</sub> to form water as a by-product. Direct methanol fuel cells (DMFCs) are a class of PEMFC, which uses methanol as the stable hydrogen source at the anode. Methanol releases six pairs of protons and electrons during oxidation which makes it a sustainable high-density fuel which is advantageous [6]. DMFCs holds huge potential and are being explored as an alternative to IC engines, for stationary and portable sources of power. The vital merit of generating high power over low voltage of a DMFC is restricted by the methanol crossover which results in non-electrochemical oxidation and internal short-circuiting of the cell [7].

The proton exchange membrane (PEM) is the heart of a fuel cell stack which acts as a bridge for the proton transfer while maintaining the barrier between the fuel and oxidant compartments, thereby, preventing them from mixing. At present, the most widely used proton exchange membrane is Nafion due to its high proton conductivity. However, it has certain drawbacks such as high methanol permeability and cost [8, 9]. Hence, researchers are keen on exploring alternative membranes for DMFCs. Various polymer materials such as poly(vinylidene fluoride) (PVDF) [10], chitosan [11], Sulfonated poly(phenylene ether ether sulfone) [12], sulfonated poly(etheretherketone) (SPEEK) [13], etc., have been investigated for their performance as proton exchange membranes. A highly efficient membrane should possess a rigid polymer backbone having ionic species that can transport protons attached to it. Consequently, sulfonated polymers have been explored and their results indicate that the hydrophilic sulfonic acid groups tend to aggregate into as nano-scale ionic complexes within the hydrophobic polymer matrixes which enhances the proton transport due via Grotthuss Mechanism, vehicular transport and surface mechanisms [14]. Though the proton conductivity was enhanced when sulfonated membranes were used, an increase in the degree of sulfonation could cause swelling of the polymer thereby permitting methanol crossover [15]. Moreover, there are free radicals produced during the operation that could eventually lead to polymer damage and diminish the membrane integrity, lowering the membrane life. In fact, a combined mechanical, thermal and chemical degradations cause membrane failure and a need for membrane replacement [16].

To overcome these limitations, nanocomposite membranes have gained significant interest; nano-fillers such as graphene oxide (GO) [17], carbon nanotubes (CNTs) [11], titanium oxide [18], layered double hydroxide [19], zirconia [20], MOF [21] have been investigated. The recent

increase in the use of nano-fillers to tailor the resulting properties of composites is due to their extensive range of physical and chemical properties. For instance, graphene has high electrical conductivity, high thermal conductivity, high specific surface area with flexible chemical properties achieved through functionalization (e.g. oxidation and sulfonation). CNTs and GO stand at the forefront of obtaining different types of polymer nanocomposites, with their application ranging from fuel cells to biosensors [22, 23]. The formation of a nanocomposite membranes takes place in two stages – dispersion of nano-filler in the polymer solution and preparation of membrane. A suitable PEM should have appropriate water uptake, low swelling ratio, dense structure, high proton conductivity, high thermal stability, good mechanical properties and chemical stability.

Poly(vinylidene fluoride) (PVDF) is chosen as the base polymer in this work as it has been widely used in the field of fuel cells owing to its excellent chemical resistance, sufficient thermal stability and outstanding mechanical properties [24].

CMK-3 is a class of mesoporous carbons which have been recently exploited due to its properties such as uniform pore size distribution, large surface to volume ratio and superior chemical stability, tailorable surface functionalities which makes it an ideal nanofiller [25]. The sulfonated, mesoporous carbon CMK-3 is incorporated into a long chain sulfonated poly(etheretherketone) (SPEEK) is used to enhance the performance of PVDF membranes to be used as a proton exchange membrane. Here, SPEEK itself promotes proton hopping due to the acid site present and it helps to anchor the sCMK-3 into the polymer matrix. This modification imparts a much greater number of ionic active sites, improves the overall proton transport, restricts swelling and thermal degradation, all of which is highly essential for membranes used for DMFCs.

The morphology, surface chemistry and strength of the novel nano-composite membranes were evaluated. The methanol crossover and proton conductivity were studied to observe the effect of sCMK-3/SPEEK on the membrane properties for low-temperature direct methanol fuel cells. These membranes can be scaled up easily for applications in DMFCs which could address the economic as well as the environmental gap in the energy sector, which is of high demand in India.

## 2 Experimental

### 2.1 Materials

PVDF (melt index 7–20 g/10 min; Mw ~ 2,75,000), raw materials for the synthesis of SBA-15 and CMK-3 were

procured from Merck. PEEK pellets were obtained as a gift sample from a Solvay India. Concentrated sulfuric acid ( $\text{H}_2\text{SO}_4$ ) (98%, Emplura) was bought from Merck Life Science Pvt. Ltd (India). N-Methyl-2-pyrrolidone (99.5% purity NMP, AR), was purchased from Sisco Research Laboratory, (India). Ethanol, absolute, was purchased from Changshu Hongsheng Fine Chemicals Co. Ltd. (China). All the materials and chemicals were of analytical grade and used as received. Clean and dried glasswares and de-ionized water were used throughout the study.

## 2.2 Preparation of CMK-3 via nano-casting method

Mesoporous silica, SBA-15 was synthesized as in our previous study [26] and used as the hard templating agent for the synthesis of CMK-3. The typical synthesis of the ordered mesoporous carbon is as follows - initially, the SBA-15 was pre-dried at 80 °C under vacuum for 3 h before use. Briefly, 1.25 g of acidified sucrose solution was mixed thoroughly with 1.0 g of SBA and the subsequent mixture was dried at 373 K for 6 h and 443 K for 6 h to obtain a partially polymerized and carbonized sucrose. The dry brown/black material was further ground and mixed with 1 g of acidified sucrose solution and dried using a similar procedure. The black mass obtained was powdered and then carbonized in a muffle furnace at 1173 K for 6 h under an inert atmosphere ( $\text{N}_2$  purge). A 5 wt% HF was used to dissolve the silica template from the obtained product at room temperature. The template-free carbon product was washed, filtered and dried for further use [27].

## 2.3 Sulfonation of PEEK and CMK-3

PEEK was directly sulfonated using sulphuric acid. 2.5 g of dried PEEK pellets was slowly added to 30 ml of concentrated sulphuric acid kept in an oil bath (80 °C) undergoing constant stirring. After the desired sulfonation of PEEK took place (2 h), the solution was slowly poured into excess deionized water at room temperature. The washing process was repeated until the solution reached ~ 7.5 pH. Finally, the so formed SPEEK was dried in a vacuum oven for 24 h at 70 °C and its ion exchange capacity was found to be 0.24 [28].

For the preparation of sCMK-3, 250 mg of mesoporous carbon was gradually added into 60 ml of concentrated sulphuric acid and was sonicated for 20 min under room temperature [29]. After thorough dissolution, the mixture was heated at an elevated temperature for 6 h. The sulfonated mesoporous carbon (sCMK-3) was washed with water/ethanol and dried in a hot air oven for further characterization.

## 2.4 Membrane preparation

A predetermined wt% of sCMK-3 was initially dispersed into a part of the solvent NMP using a sonication bath, following which a known quantity of SPEEK was dissolved by stirring at 45 °C. The PVDF powder was added to the remaining part of the solvent dissolution was carried out by mechanical stirring at room temperature. The two parts were mixed under constant stirring until the solution appeared homogenous. The homogenous dope solution was degassed using a vacuum pump. The dope solution was cast on a clean dust-free glass plate at room temperature using a semi-automatic casting unit (Elcometer 4340). The spread film was dried in a hot air oven at 80 °C for 24 h. To further remove the residual solvent, the membranes were kept immersed in a water bath for 24 h and the compositions of the membranes are given in Table 1.

## 2.5 Characterization of sCMK-3 and membranes

The morphology and structure of the mesoporous particles were investigated using a transmission electron microscope (TEM, JEOL JSM-2100F) and a field emission scanning electron microscopy (FESEM, VEGA3 TESCAN) at an accelerating voltage of 15 kV. The small-angle X-ray diffraction (XRD) patterns of the samples were recorded on a powder diffraction-meter (SAXRD, BRUKER D8 FOCUS), operating with Cu K $\alpha$  radiation ( $\lambda = 1.54 \text{ \AA}$ ) at 25 kV and 40 mA in the  $2\theta$  range of  $0.6^\circ$ – $10^\circ$ . Wide angle XRD patterns of the samples were measured in the  $2\theta$  range of  $10^\circ$ – $80^\circ$ . Fourier transform infrared spectroscopy (FT-IR, BRUKER) within the wavenumber range of  $400$ – $4500 \text{ cm}^{-1}$  was carried out to determine the chemical structure of the materials. The Raman spectra were collected using Raman spectrometer (iRaman plus, B&W TEK) using a 532 nm laser line as the excitation source.

**Table 1** Composition and properties of the prepared membranes

Membrane code	Membrane casting composition (wt%)		Water uptake at 45 °C (%)	Swelling ratio at 45 °C (%)	IEC ( $\text{meq g}^{-1}$ )
	SPEEK	sCMK-3			
M0	0	0	04.25	0	–
M1	0	0.025	12.08	1.20	0.38
M2	4	0.025	23.47	10.36	0.92
M3	6	0.05	37.80	22.74	1.82
M4	4	0.05	33.60	14.73	1.76
M5	6	0	39.50	28.34	1.69

Total polymer concentration (PVDF + SPEEK) was always maintained at 14 wt% of the total mixture. NMP was used as the solvent for preparation of the membranes

The nitrogen adsorption–desorption isotherms were obtained at 77 K on a Belsorp Max (BEL, Japan) instrument, after degassing the samples at 180 °C and  $10^{-4}$  Pa for 3 h. The specific surface area of the samples was evaluated by the Brunaur–Emmet–Teller (BET) method, and pore size distribution curves were calculated using the Barrett–Joyner–Halenda (BJH) method. Pore volume and average pore size were obtained according to the  $N_2$  adsorption volume at  $P/P_0 = 0.97$

Cross section and top surface morphology were obtained by SEM imaging utilizing a Field emission scanning electron microscopy (FESEM, VEGA3 TESCAN). An atomic force microscope (Nanosurf EasyScan 2 AFM) was used to image the surface roughness of the membranes and was carried out in a non-contact mode ( $n = 5$ ). ATR-FTIR was carried out using, Bruker Alpha-T. The surface wettability was evaluated using the sessile drop method using a goniometer type contact angle instrument ( $n = 8$ ; Ramé-Hart Model 250, USA)

The mechanical properties of the membranes were measured at room temperature using a universal testing machine (INSTRON 2519-104) with a maximum stretching load of 500 N. Dumbbell-shaped specimens of gauge dimensions according to ASTM D3039 were used and the tests were carried out at a rate of 2 mm/min. For each measurement, four specimens were tested and their average value was reported. The thermal stability of the membranes was analyzed using the Thermogravimetric analysis (TGA) using a STA7200RV, Hitachi High-Technologies and the temperature was increased from 25 to 700 °C at a rate of 10 °C/min. An atomic force microscope (Nanosurf EasyScan 2 AFM) was used to image the surface roughness of the membranes and was carried out in a non-contact mode ( $n = 5$ ).

## 2.6 Water uptake (WU) and swelling ratio (SR)

The hydrophilicity of the membranes was studied using the WU and SR measurements. The membrane samples were first dried in a hot air oven at 80 °C until both the measured weight ( $W_{dry}$ , g) and the thickness ( $T_{dry}$ , mm) was constant. After which, the dry samples were soaked in water at room temperature until fully hydrated. Excess water was wiped off using filter paper, and the weight ( $W_{wet}$ , g) and thickness ( $T_{wet}$ , mm) of the hydrated membranes were measured. The water uptake and area swelling were then calculated by the following equations ( $n = 3$ ),

$$\text{Water uptake (\%)} = \frac{W_{wet} - W_{dry}}{W_{dry}} \times 100 \quad (1)$$

$$\text{Swelling ratio (\%)} = \frac{T_{wet} - T_{dry}}{T_{dry}} \times 100 \quad (2)$$

## 2.7 Proton conductivity and Ion-exchange capacity (IEC) of the membranes

AC impedance technique was used to determine the resistance of the membranes (Autolab Potentiostat Galvanostat PGSTAT-30) in the frequency range of 1 Hz to  $10^5$  Hz with an oscillating voltage of 10 mV.

The membranes were initially hydrated by soaking them in de-ionized water before they were loaded between two stainless steel electrodes. The resistance of the membranes was calculated from the intercept with the  $Z_{real}$  from the Nyquist plots [30]. The proton conductivity of the membrane was calculated at 45 °C from,

$$\text{Proton conductivity } (\sigma) = \frac{T}{\Omega A} \quad (3)$$

where  $T$  is the thickness of the membrane (cm),  $R$  is the membrane resistance ( $\Omega$ ) and the  $A$  is the effective surface area exposed to proton transfer ( $\text{cm}^2$ ).

To determine the ion exchange capacity of the membranes a 2 cm × 2 cm sample was placed in a 2 M NaCl solution to induce the liberation of  $H^+$  ions. The solution was then titrated against 0.1 N NaOH solution using a phenolphthalein indicator. The IECs of the prepared polymeric membranes were calculated with the following equation ( $n = 3$ ),

$$\text{IEC} \left( \frac{\text{meq}}{\text{g}} \right) = \frac{N \times V}{W_{dry}} \quad (4)$$

where  $N$  is the normality of NaOH,  $V$  is the titre volume of NaOH consumed and  $W_{dry}$  is the weight of the dry membranes [31].

## 2.8 Methanol permeability

The methanol permeability was determined by using a homemade diffusion cell comprising of two compartments, each of volume 30 ml. 2 M methanol was placed in one compartment (A) and de-ionized water in the other (B). The membrane was fixed between the junction of the two compartments using a highly porous support. Both cells were stirred continuously throughout the experiment. The concentration of methanol diffused was determined using a gas chromatograph (Shimadzu GC-17A) equipped with a ZB-FFAP capillary column and a flame ionization detector (FID). The methanol permeability was calculated using the following equation ( $n = 3$ ),

$$P = \frac{ST}{AC_{A0}} V_B \quad (5)$$

where  $C_{A0}$  is the initial concentration of methanol taken in the feed.  $A$ ,  $T$ ,  $V_B$  represent the effective area, the thickness

of the membrane and the volume of methanol which has diffused from compartment A to B.  $S$  represents the linear slope of methanol concentration in the water compartment versus time [32].

### 3 Results and discussion

#### 3.1 Characterization of sCMK-3

The SEM image (Fig. 1a) confirms the worm/rod-shaped morphology is unaltered for the sCMK-3. This suggests that the bulk structure does not get impacted when treated in acidic conditions at elevated temperatures [33]. The FTIR spectrum of pristine CMK-3 (Fig. 1b) shows no functional groups except a water absorption band at  $\sim 3430\text{ cm}^{-1}$ . The water absorption peak was more intense owing to the O–H stretching vibrations of a greater number of water molecules present in sCMK-3. The S=O symmetric

stretching vibrations were observed at  $1018\text{ cm}^{-1}$  and the peak at  $1388\text{ cm}^{-1}$  corresponds to the asymmetric  $\text{SO}_2$  stretching in  $\text{SO}_3\text{H}$  [34]. This confirms the successful sulfonation of CMK-3 without any structural deformation.

The small angle XRD spectra were recorded to determine the degree of structural order. CMK-3 exhibits a strong diffraction peak corresponding to the (100) plane and 2 low-intensity distinct peaks of the (110) and (200) plane reflections, exhibiting a hexagonal  $P6\text{ mm}$  space group, as seen from Fig. 1c. The impregnation of sucrose is carried out twice in the nano-casting which leads to the formation of well-developed carbon spacers between the carbon rods. Moreover, the microporous present in the SBA-15 helps stabilize the inverse carbon template. The three distinct peaks with lower intensities are present in the sulfonated CMK-3, with a small right shift of the (100) plane reflection. It can be confirmed that using mesoporous carbon material results in only a diminutive increment in the disorder of the structure and a minor

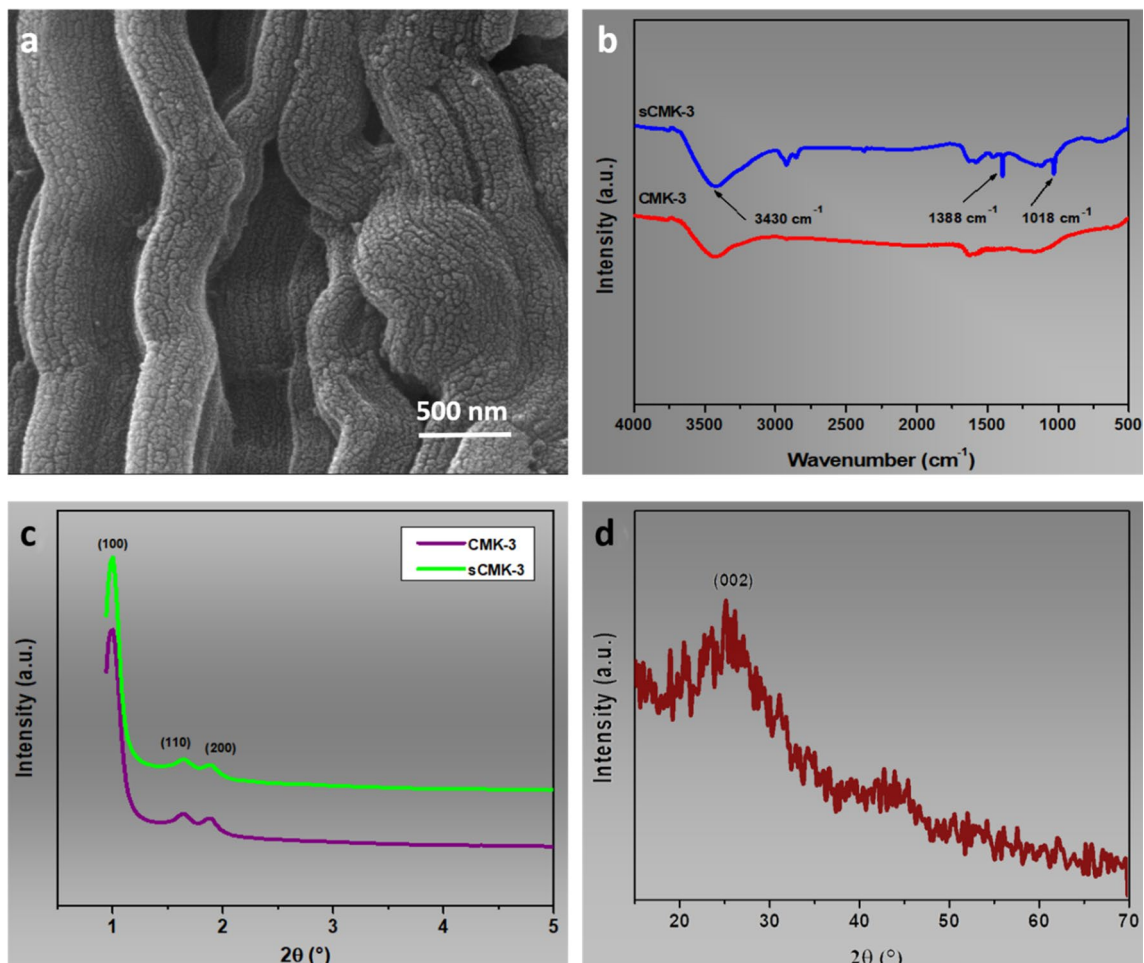


**Fig. 1** Sulfonated mesoporous carbon (sCMK-3): **a** HR-SEM (morphology), **b** FT-IR spectra (chemical structure) and **c**, **d** low and wide angle X-ray diffraction patterns

shrinkage of the framework. The formation of additional micropores during the heat treatment was avoided and its original 2-D hexagonal structure was well maintained [35].

The wide-angle XRD spectrum of sCMK-3 Fig. 1d displays the two broad typical diffraction peaks at  $2\theta = 23^\circ$  and  $43^\circ$  corresponding to the (002) and (101) planes, suggesting the low graphitized material [36] similar to that of CMK-3.

The successful preparation of CMK-3 via the nano-casting method using SBA-15 was confirmed by the homogenous micrometer-sized worm/rod-like structure in the TEM image (Fig. 2). The powder samples viewed perpendicular to its hexagonal pore arrangement exhibited ordered mesoporous structure with uniform parallel pores, as seen from Fig. 2. The white parallel lines correspond to the mesopores that are generated wherein the walls of the template SBA-15 was formerly present [37]. As seen in Fig. 2d, e, sCMK-3 retains the uniformity of the mesopores of the original inorganic wall structure of the parent CMK-3 carbon. Figure 2f, is the representation of the distance between the walls of the CMK-3 (indicated by a yellow line in Fig. 2e). The result indicates that the sulfonic acid groups do not alter the structure of the mesoporous carbon CMK-3 and also the even spacing of

long parallel mesoporous structure proving no defect in the morphology of the sCMK-3.

The Raman spectra (Fig. 3), illustrates 2 distinct peaks at  $1334\text{ cm}^{-1}$ ,  $1590\text{ cm}^{-1}$  corresponding to the D-band and G-band respectively. The G band is due to the vibrations arising from the in-plane stretching between the  $sp^2$  hybridized C–C ( $E_{2g}$  vibration band); whereas the D band arises due to the  $sp^3$  hybridized carbon that occurs due to the partially disordered structure of carbon backbone. There is a small blue-shift of the D and G bands to  $1332.7\text{ cm}^{-1}$ ,  $1602\text{ cm}^{-1}$  sCMK-3 with a slight increase in  $I_D/I_G$  ratio (1.08–1.12) [38].

In the range of  $P/P_0 = 0.4\text{--}0.6$  both CMK-3 and sCMK-3 show condensation in the adsorption–desorption isotherm indicating it to be a type IV isotherm according to IUPAC classification (Fig. 4). These particles had an H1 type of hysteresis loop indicating a mesoporous structure with long, uniform cylindrical pores.

A higher surface area and pore volume of  $789.2\text{ m}^2\text{ g}^{-1}$  and  $182.6\text{ cm}^3\text{ g}^{-1}$  were exhibited by CMK-3 and whereas,  $765.23\text{ m}^2\text{ g}^{-1}$  and  $175.82\text{ cm}^3\text{ g}^{-1}$  was observed for sCMK-3. This decrease in surface area and pore volume confirms the successful incorporation of  $-\text{SO}_3\text{H}$  groups into the CMK-3 matrix. The pore size determined by the

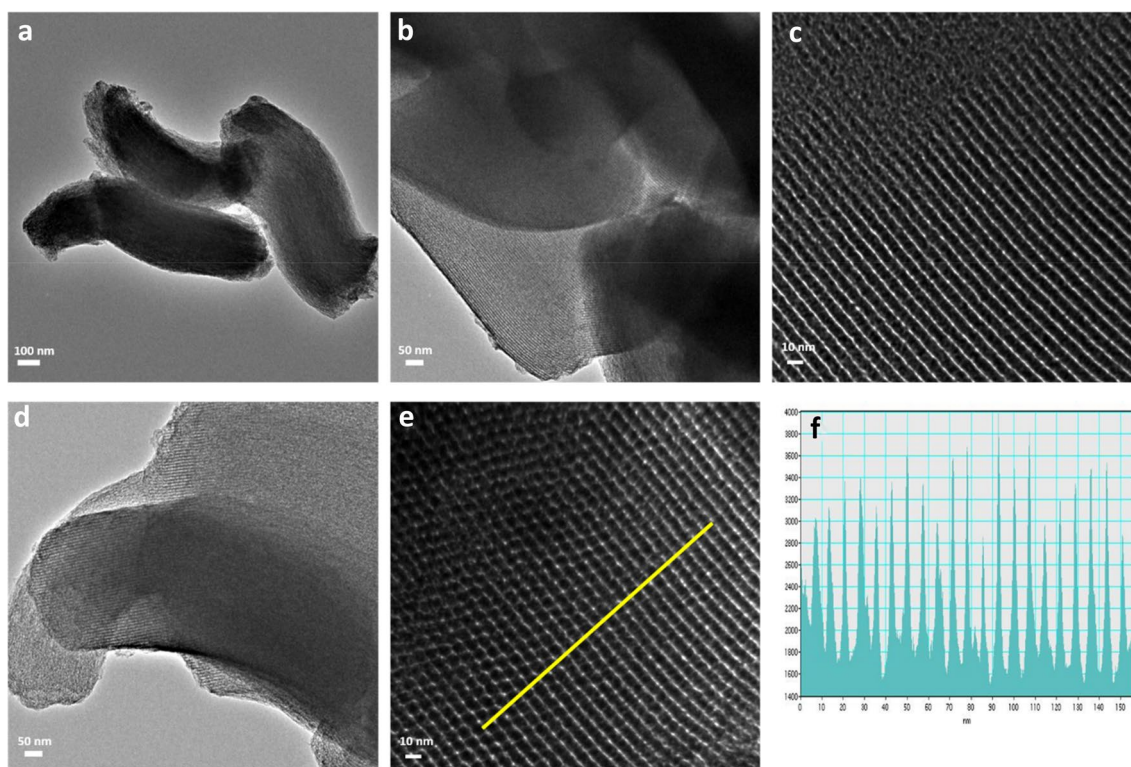


**Fig. 2** HR-TEM images: **a–c** nano-casted mesoporous carbon (CMK-3), **d, e** sulfonated mesoporous carbon (sCMK-3), **f** corresponding width of the mesoporous channels

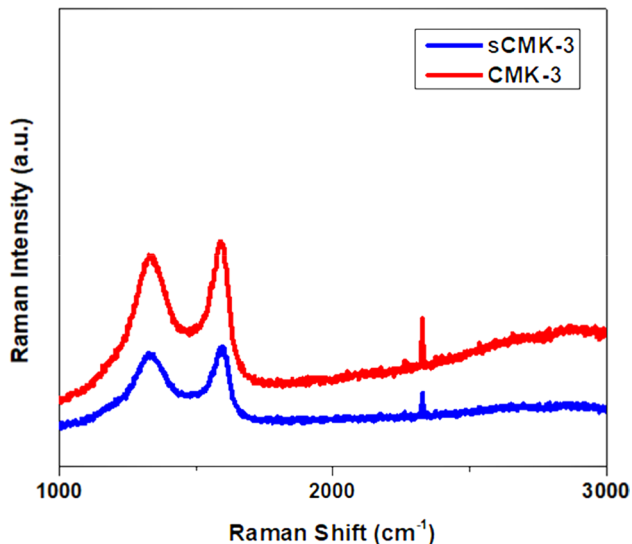


Fig. 3 Raman shift of the sCMK-3

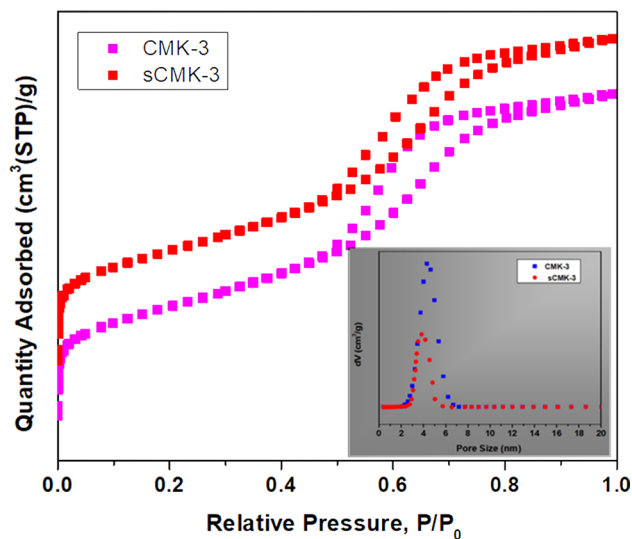


Fig. 4 The absorption–desorption hysteresis from BET analysis and the pore size distribution of the mesoporous materials (inset)

BJH method, calculated a decrease in mean pore diameter from 5.43 to 5.21 nm [29].

The bulk composition of CMK-3 obtained by the XRF analysis did not present any S content and only a low oxygen content (2.7%) which could have been incorporated during the synthesis of CMK-3. The sulfonated mesoporous CMK-3 had an increase in sulfur concentration (9.2%) and a corresponding increase in oxygen as  $\text{SO}_3$ . The XRF analysis further confirms the sulfonation of the sCMK-3 and also quantifies the incorporation of the sulfonic acid group.

## 3.2 Characteristics of the prepared membranes

A preliminary physical characteristic, its optical appearance could be used to differentiate the prepared membranes. The pure PVDF membrane was observed to be translucent and having a white colour. Incorporation of SPEEK (M5) into the PVDF matrix changed the colour to pale yellow. Incorporation of the sCMK-3/SPEEK nanocomposite imparted a grey/black tinge which also confirms the uniform dispersion of the nanofiller.

### 3.2.1 Chemical structure of the membranes

From Fig. 5, it can be seen that the pristine M0 membrane exhibits characteristic vibrations at  $1174\text{ cm}^{-1}$  and  $1209\text{ cm}^{-1}$  which is attributed to the asymmetric and symmetric stretching of the  $-\text{CF}_2$  respectively. Another prominent peak at  $1404\text{ cm}^{-1}$  is due to the vibrations of the difluoromethylene groups [39]. Membranes M3, M4 showed the characteristic peaks of SPEEK which included the carbonyl stretching vibration at  $1653\text{ cm}^{-1}$ , the skeletal ring vibration at 1593, 1500, 1485 and  $1410\text{ cm}^{-1}$ , a number of aromatic hydrogens in-plane deformation bands at 1215, 1155 and  $1010\text{ cm}^{-1}$ , the diphenyl ketone band at  $925\text{ cm}^{-1}$ , the out of plane bending modes of the aromatic hydrogens (two overlapping broad bands) at 863 and  $841\text{ cm}^{-1}$  and a band at  $765\text{ cm}^{-1}$  [40]. In addition, the broad band at  $\sim 3450\text{ cm}^{-1}$  due to the presence of the  $-\text{OH}$  bonds is an indication of the incorporation of  $-\text{SO}_3\text{H}$  groups on the membrane surface. The peaks at  $1083\text{ cm}^{-1}$  and  $1256\text{ cm}^{-1}$  correspond to the symmetric vibrations

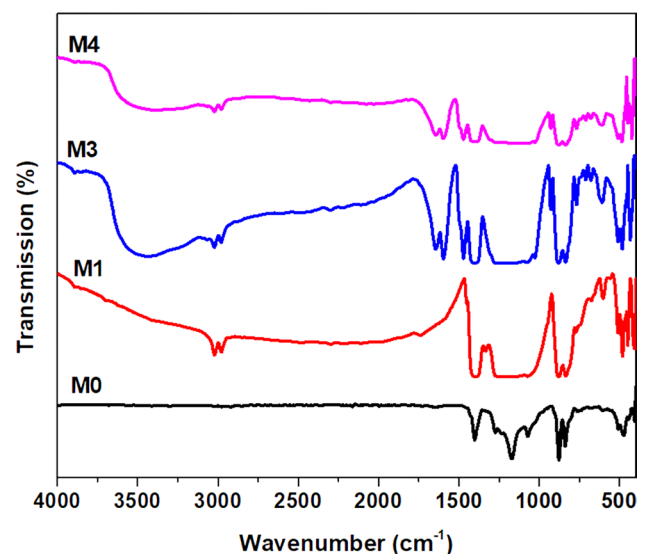


Fig. 5 Fourier transform infrared spectroscopy analysis of the fabricated membranes

and asymmetric vibrations of the O=S=O groups of the sCMK-3/SPEEK nanocomposite.

### 3.2.2 Water uptake and swelling ratio

Water uptake is a critical factor which determines the proton conductivity of the membrane. The water content in the membrane creates specific channels for the protons to be transported from the anode chamber to the cathode chamber. The membrane's ability to uptake water increases its proton conductivity and this WU must be limited so as to prevent membrane swelling that in turn causes a dimensional instability in the membrane electrode assembly [41].

The swelling ratio of a PEM is another equally important parameter as it corresponds to the membrane's structural integrity. It is observed that higher water uptake improves the ionic conductivity of the membrane. However, the water molecules have a plasticizing effect on the membrane which decreases its mechanical stability. Moreover, these dimensional instabilities will lead to the separation of the membrane from the electrodes, which would give rise to an electrochemical instability of the MEA [42, 43].

Table 1 shows the WU and SR of the prepared membranes, the incorporation of increasing concentrations of hydrophilic SPEEK and sCMK-3 impart the membrane with enhanced water uptake as well as swelling ratio. The membrane M4 exhibited sufficiently high WU of 33.6% and only a moderate swelling ratio due to the incorporation of the nanocomposite. However, M5, displayed the maximum SR of 28.34% which could be detrimental in membrane electrode assembly and can be attributed to the incorporation of SPEEK. The presence of sCMK-3 in the nanocomposite incorporated membranes is seen to restrict the swelling of the polymeric chains.

### 3.2.3 Membrane morphology-field emission scanning electron microscopy and atomic force microscopy

Scanning electron microscopy was used to investigate the top-surface and cross-sectional morphology of the prepared PEMs. The dried pristine PVDF membranes exhibited micro-fissures and the incorporation of the nanocomposite is seen to have altered the membrane architecture. Incorporation of a small quantity of sCMK-3 did not greatly influence the top surface morphology.

However, incorporation of greater quantities of SPEEK drastically transforms the membrane's top surface introducing much greater pore openings which could explain the increase in methanol permeability seen in the latter section. Incorporation of sCMK-3/SPEEK nanocomposite displayed wrinkles and much lower pore openings and

moreover, no apparent aggregation of the nanofillers was observed (Fig. 6).

The distribution of the mesoporous sCMK-3 within the membrane matrix has a great influence on the cross-sectional morphology of the prepared membranes. The cross-sectional images (Fig. 7) given in fig display a dense substructure for the pristine PVDF membrane, which corroborates the results of low porosity. The visible increase of microporosity in the substructure can act as the domains of water molecules which aid the transport of protons across the membrane surface. Moreover, the favourable dispersion of the nanocomposite with high density  $-SO_3H$  would also enhance proton transport.

AFM is a tool which is used to investigate the phase morphology of a sample using different properties such as, hardness, modulus and the roughness of the surface. The incorporation of the nanocomposite is seen to alter the surface of the membranes increasing the surface roughness. The formation of hydrogen bonds between the sulfonic acid groups of the sCMK-3 and the SPEEK leads to the creation of rougher surfaces [43]. Increase in the SPEEK content significantly contributes to the changes in surface morphology (Fig. 8).

The rougher surfaces provide increased surface area for the proton conduction and promote the formation of hydrated proton conduction channels especially at high water retention capacity. The presence of acidic groups increases the rate of solvent/non-solvent exchange during the phase inversion process due to its ability to act both as an H-bond donor and acceptor. Hydrophilic membranes with increased surface roughness increase the surface area and produce channels for proton migration [44].

### 3.2.4 Surface wettability

The hydrophobic-hydrophilic balance of the membrane electrode assembly affects the performance of the membranes. The cathode catalyst layer is designed to be hydrophobic to prevent the flooding of the catalyst layer and the subsequent loss of catalyst activity. However, the proton exchange membrane requires water moieties to enhance the transport of  $H^+$  ions [45]. It could be seen that the pristine PVDF membrane exhibited the lowest wetting as characterized by the highest water contact angle of  $95.2^\circ$  (Fig. 9), this could be due to the smoother surface as well as non-availability of any polar groups. Low concentration of sCMK-3 (M1) only slightly improved the membrane hydrophilicity. It can be observed that the incorporation of sCMK-3/SPEEK nanocomposite into the membrane matrix caused an appreciable decline of the water contact angle. This could be explained as the synergistic effect of the sulfonic acid moieties at the membrane surface, the increased surface porosity as well as the enhanced surface



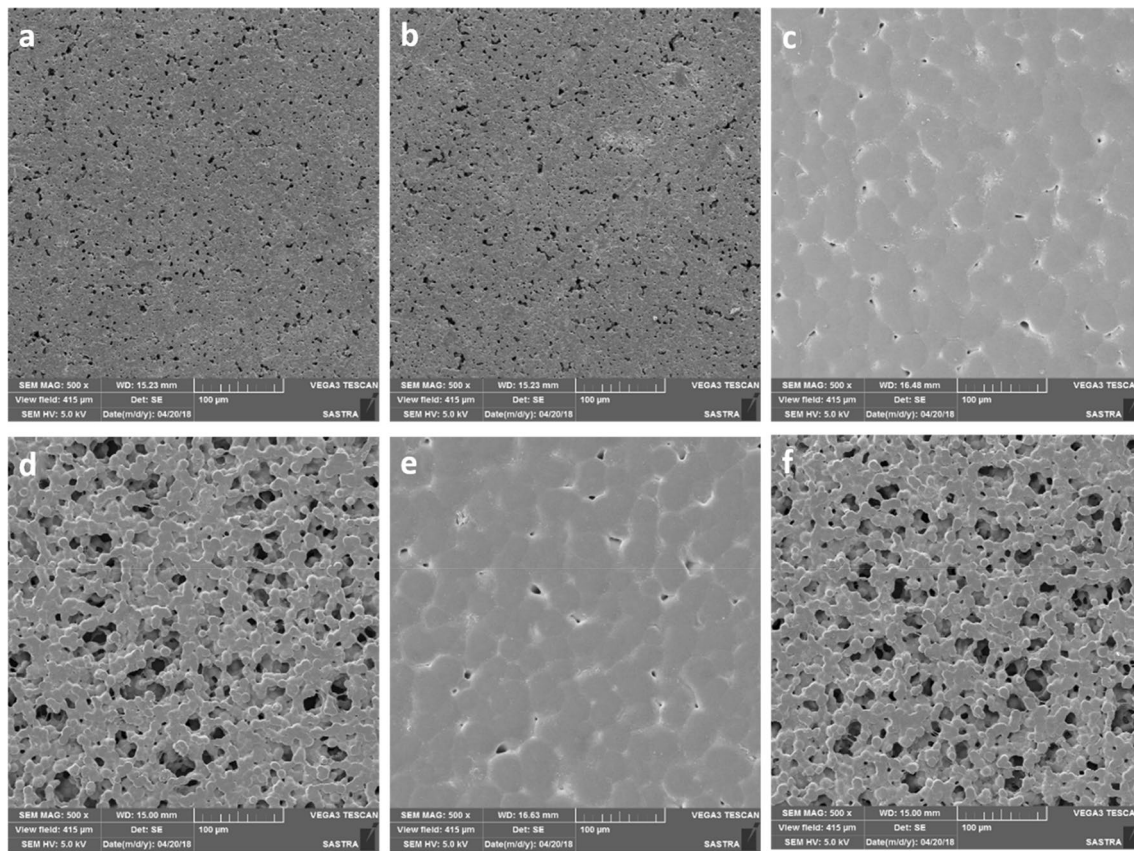


**Fig. 6** Top surface morphology of the membranes using SEM imaging **a** M0, **b** M1, **c** M2, **d** M3, **e** M4 and **f** M5

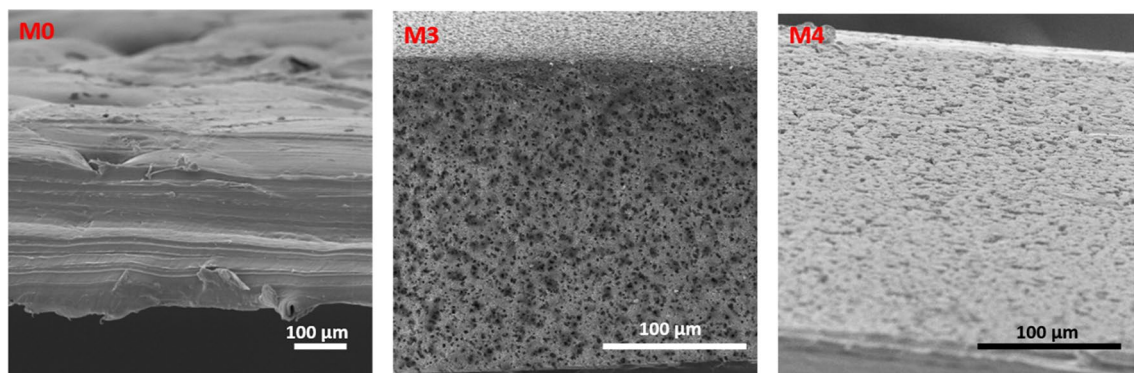


**Fig. 7** Cross-section morphology of the prepared membranes using SEM imaging

roughness of the membranes. These factors contribute to the improvement in the hydrophilic nature of the membrane which is essential in the proton conduction through the membrane electrode assembly.

### 3.2.5 Thermal analysis and stability

The stability of the prepared membranes and their degradation are important if the membranes are to be used at

higher temperatures, as it enhances the overall membrane performance. The thermogravimetric analysis of the pristine PVDF membrane and membranes incorporated with the sCMK-3/SPEEK nanocomposite were carried out under inert atmosphere and the thermograms are presented in Fig. 10.

M0 shows a characteristic single-step degradation pattern as observed in earlier works. The PVDF is a homopolymer containing  $-CF_2$  groups and is stable

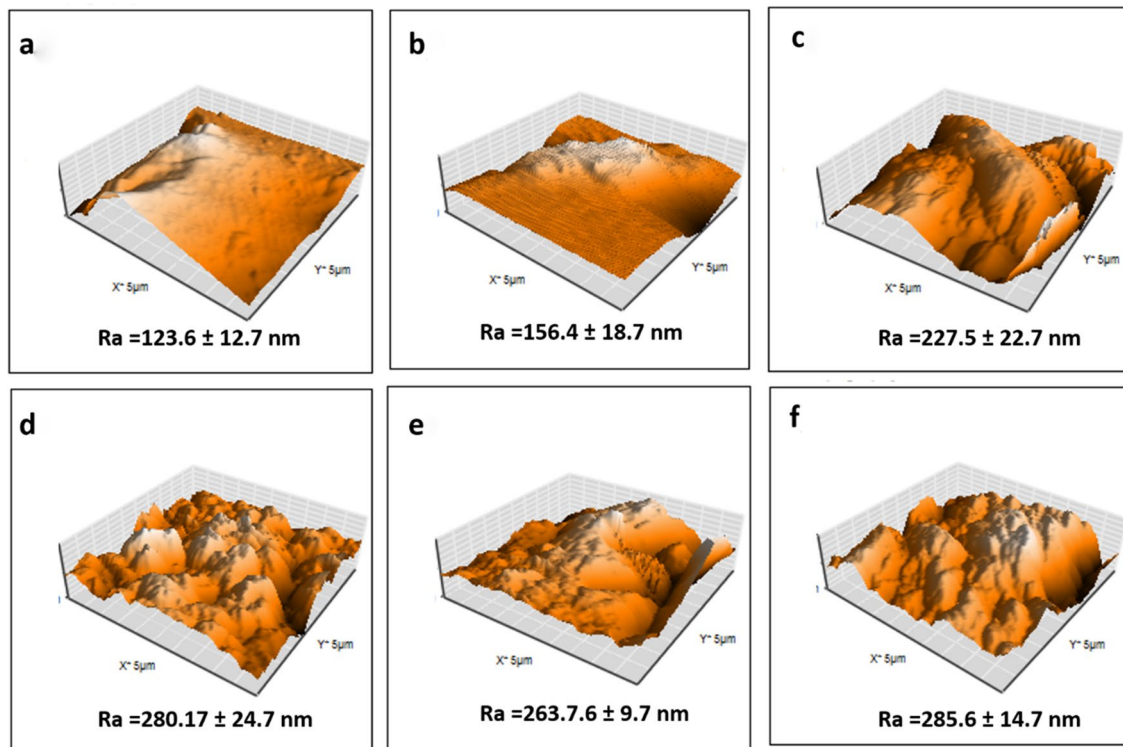


**Fig. 8** Three dimensional surface morphology of the membranes **a** M0, **b** M1, **c** M2, **d** M3, **e** M4 and **f** M5 and their average surface roughness

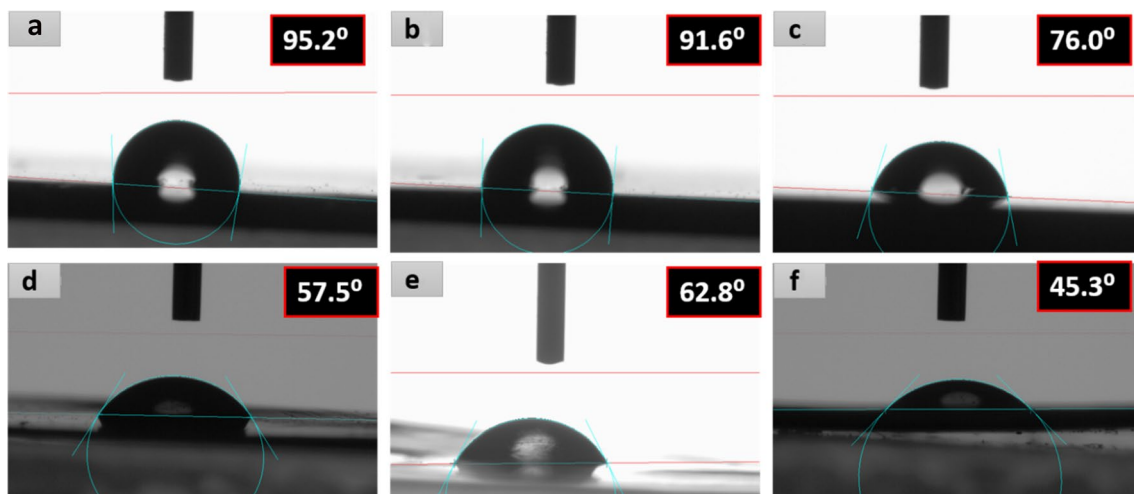


**Fig. 9** Water contact angle images of membranes **a** M0, **b** M1, **c** M2, **d** M3, **e** M4 and **f** M5

up to  $\sim 370$  °C and a weight loss of  $< 6\%$  is observed between 425 and 480 °C which is attributed to the degradation of the PVDF backbone [46]. Incorporation of the nanocomposite does not deteriorate the thermal stability of the membrane matrix and has a small increase in the degradation temperature. The DTG also shows no

other degradation step and no loss due to degradation of SPEEK.

No weight losses can be observed for membranes M3 and M4 which confirms that the mesoporous carbon material was well dispersed and anchored with the SPEEK polymer. The formation of a greater number of H-bonding

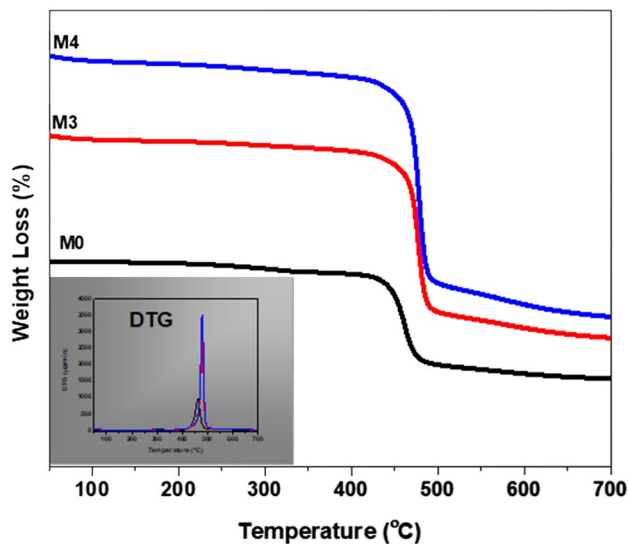


**Fig. 10** Temperature dependent weight loss using thermogravimetric analysis and the DTG curves (inset)

between the sulfonic acid moieties also played a role in the thermal stability of the membranes. This shows that these membranes can be tested for its performance efficiency even at higher temperatures.

### 3.2.6 Mechanical properties of the membranes

The mechanical properties of the PEM's were tested to ensure their successful candidature for DMFC application. The mechanical performances of fully hydrated membranes are poorer compared to the dry membranes, at the same temperature and humidity. For the fully hydrated membranes, the membranes swell after water absorption, the intermolecular gap becomes larger and the interaction force becomes weaker, leading to decreased mechanical stability.

The mechanical properties were measured at room temperature and the results are indicated in Table 2. As seen from the table, the addition of sCMK-3 increases the tensile strength of the nano-composite incorporated membranes, indicating a strong interaction of the nanofiller with the polymer matrix. This overall increase in the mechanical property of the membranes is due to the strong hydrogen bonding between the nanofiller and the polymer matrix, which increases the compactness and enhances the mechanical stability of the membrane [47].

Membrane M4 exhibits the greatest mechanical stability due to high inter-hydrogen bonding between the  $\text{SO}_3\text{H}$  groups,  $\text{C}=\text{O}$  and oxygen groups and oxygen atoms of the sCMK-3/SPEEK nanocomposite, which is even greater than commercial Nafion 117 [48]. It is found that membranes with a SPEEK concentration greater than

**Table 2** Mechanical properties and selectivity of the membranes

Membrane	Tensile strength (MPa)	Tensile strain at Maximum Tensile extension (mm/mm)	Membrane selectivity ( $\text{S cm}^{-3}$ )
M0	759.50	0.040	$0.0537 \times 10^4$
M1	841.29	0.052	$2.6936 \times 10^4$
M2	826.34	0.062	$2.4472 \times 10^5$
M3	687.5	0.058	$1.6135 \times 10^4$
M4	862.2	0.071	$8.2949 \times 10^5$
M5	501.09	0.047	$8.044 \times 10^4$

4% possessed lower tensile strength which could be explained by the lower miscibility of the SPEEK with the PVDF backbone as observed for membranes M3 and M5.

### 3.3 Proton conductivity and Ion exchange capacity (IEC) of the membranes

The IEC is one of the critical parameters which determines the transport property of the membrane. It is an indication of the number of exchangeable ions present and represents the fraction of hydrophilic moieties present in the membrane sample. All modified membranes possess higher IEC compared to pristine PVDF membrane. The increase in IEC values (Table 1) may be attributed to the presence of hydrophilic acidic sites in SPEEK and CMK-3 which is thought to be responsible for improving the water retention that promotes the proton hopping even in low humid conditions. Sulfonation provides a large number of  $-\text{SO}_3\text{H}$  moieties which become the domain of water molecules that form interconnected hydrated networks which promote the Grotthuss type of proton transfer through the membrane [49].

Proton conductivity was measured by impedance spectroscopy and is the most significant parameter which assesses the suitability of the membrane to be employed as a proton exchange membrane. The acid sites were initially activated by soaking the membranes in de-ionized water to completely hydrate them to provide better efficiency. From Fig. 11, we can observe the proton conductivity increases with an increase in weight ratios of SPEEK and sCMK-3 in the membrane matrix. As seen in the figure, M3 has the highest proton conductivity with  $0.081 \text{ Scm}^{-1}$  and M0 with the least proton conductivity of  $0.0001 \text{ Scm}^{-1}$ , which clearly indicates the influence of the  $-\text{SO}_3\text{H}$  groups in proton conduction. Scheme 1 is a representation of the proton conduction through the membrane matrix. The results were

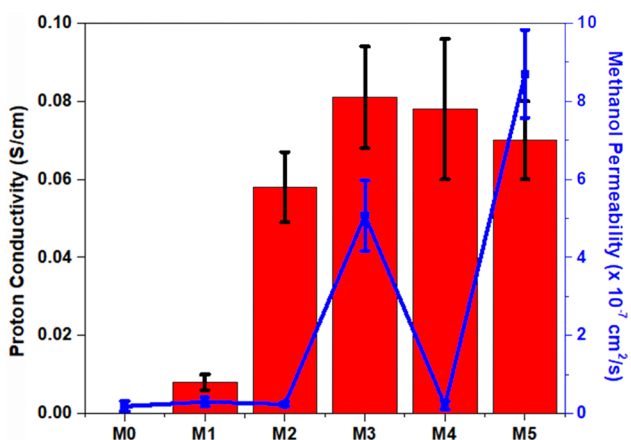


Fig. 11 Through-plane proton conductivity and methanol permeability through the prepared membranes

consistent with the incorporation of other sulfonated carbon materials like Sulfonated Graphene oxide.

### 3.4 Methanol permeability

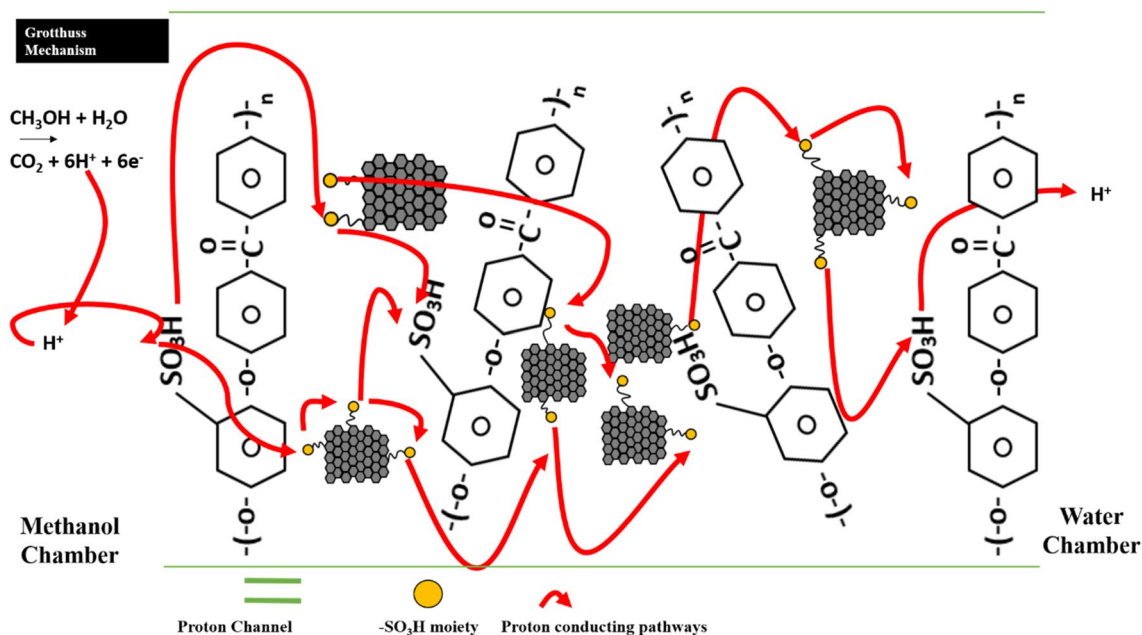
The methanol permeability is computed as the product of the diffusion coefficient and the sorption coefficient and is used to describe the motion on permeant (methanol) through the membrane matrix. The diffusion coefficient addresses the effect of the surroundings on the molecular motion of the permeant and the sorption coefficient correlates the concentration of the component in fluid phase

with its concentration in the polymer phase (membrane matrix). It is reasonable to say that the methanol permeability through our prepared porous membranes is more kinetic driven and it is hence a function of diffusion as opposed to sorption [50].

The major drawback of any DMFC is the methanol crossover, which disrupts the current density of the fuel cell stack. Methanol has to be effectively contained in the anodic chamber and its crossover to the cathodic chamber should be prevented because of its effects on low fuel efficiency and diminished cathode activity due to the mixed potential effect and the mass transfer effect at the cathode [51].

The high methanol cross over of the popular Nafion 117 is a major reason for exploring suitable alternatives [52]. As shown in Fig. 11, it can be observed that the incorporation of the sCMK-3 decreased the methanol permeability of the membrane as observed by other reports incorporating SGO into the membrane matrix [53]. M0 had a methanol permeability of  $1.86 \times 10^{-7} \text{ cm}^2 \text{ s}^{-1}$ , whereas M5 had the maximum methanol permeability with  $87.02 \times 10^{-7} \text{ cm}^2 \text{ s}^{-1}$  which confirms that the presence of porous well-developed channels.

The presence of sCMK-3 in the nanocomposite restricts the methanol crossover due to its strong interfacial occupancy of the available polymer sites [54]. The increased tortuosity, as well as the narrower pores confirmed by SEM image, also plays a vital role in hindering the methanol permeability. The methanol permeability of the membrane



Scheme 1 A graphical representation of the proton transport through the membrane matrix

**Table 3** Summary of the state-of-the-art membranes used as PEMs

S. no.	Membrane	IEC	Proton conductivity	Methanol permeability	Ref.
1.	Nafion 117	0.80 meq g <sup>-1</sup>	0.0302 S cm <sup>-1</sup>	12.2 × 10 <sup>-7</sup> cm <sup>2</sup> s <sup>-1</sup>	[55]
2.	SPEEK + graphitic carbon nitride (0.5 wt%)	1.833 mmol g <sup>-1</sup>	0.039 S cm <sup>-1</sup>	5.035 × 10 <sup>-7</sup> cm <sup>2</sup> s <sup>-1</sup>	[56]
3.	SPEEK + SPVDF-co-HFP + LaCrO <sub>3</sub> (2 wt%)	1.09 meq g <sup>-1</sup>	0.0684 S cm <sup>-1</sup>	1.87 × 10 <sup>-7</sup> cm <sup>2</sup> s <sup>-1</sup>	[57]
4.	SPEEK + sulfonated holey graphene oxide (SHGO)	1.941 meq g <sup>-1</sup>	0.0905 S cm <sup>-1</sup>	38.3 × 10 <sup>-7</sup> cm <sup>2</sup> s <sup>-1</sup>	[58]
5.	Na on-NPC (1.0 wt%)	0.82 mmol g <sup>-1</sup>	0.0751 S cm <sup>-1</sup>	9.8 × 10 <sup>-7</sup> cm <sup>2</sup> s <sup>-1</sup>	[59]
6.	SPEN + SGO (2 wt%)	1.878 mmol g <sup>-1</sup>	0.098 S cm <sup>-1</sup>	2.8 × 10 <sup>-7</sup> cm <sup>2</sup> s <sup>-1</sup>	[60]
7.	Nafion + SNPAEK (10.0 wt%)	0.78 meq g <sup>-1</sup>	0.075 S cm <sup>-1</sup>	13.65 × 10 <sup>-7</sup> cm <sup>2</sup> s <sup>-1</sup>	[61]
8.	Nafion + CNT@SiO <sub>2</sub> -PWA (1%)	0.931 meq g <sup>-1</sup>	0.087 S cm <sup>-1</sup>	2.63 × 10 <sup>-7</sup> cm <sup>2</sup> s <sup>-1</sup>	[62]
9.	sPP:sBPAES	1.99 meq g <sup>-1</sup>	0.130 S cm <sup>-1</sup>	Within limit	[63]
10.	SPEEK + Fe <sub>3</sub> O <sub>4</sub> @TDI@TiO <sub>2</sub> -SO <sub>3</sub> H	1.06 meq g <sup>-1</sup>	0.081 S cm <sup>-1</sup>	3.35 × 10 <sup>-7</sup> cm <sup>2</sup> s <sup>-1</sup>	[64]
11.	SPEEK + BPPO (20 wt%)	1.21	0.0166 S cm <sup>-1</sup>	1.39 × 10 <sup>-7</sup> cm <sup>2</sup> s <sup>-1</sup>	[65]
12.	sPVDF-HFP (18%)	0.78	0.041 S cm <sup>-1</sup>	4.61 × 10 <sup>-7</sup> cm <sup>2</sup> s <sup>-1</sup>	[63]
13.	PVDF/SPEEK-sCMK-3	1.76 meq g <sup>-1</sup>	0.081 S cm <sup>-1</sup>	2.17 × 10 <sup>-8</sup> cm <sup>2</sup> s <sup>-1</sup>	This work

M4 is 2.17 × 10<sup>-8</sup> cm<sup>2</sup> s<sup>-1</sup>, which was the least among all the nanocomposite PEM's tested.

The presence of sCMK-3 in the nanocomposite and its interaction with the base polymer, PVDF as in M4, produces the ideal PEM (increased tortuosity, narrow channels for methanol transport due to hydrogen bonding between sulfonic acid groups in SPEEK and sCMK-3) required for DMFC application.

### 3.5 Membrane selectivity and hydrolytic stability

The membrane selectivity is the ratio of the proton conductivity of a membrane to its methanol permeability and is a measure of the performance efficiency of the PEMs. The low permeability of methanol through the nanocomposite incorporated membranes is due to the low affinity of methanol due to the hydrophobic backbone of the membranes as well as some possible obstruction that is due to the presence of sCMK-3 which hinder the movement of methanol.

A pore obstruction, which reduces the methanol permeability also can reduce movement of water moieties which leads to a flux decline as observed in some earlier reports [55]. However, from Table 2 we can observe that membranes M2 and M4 exhibits the greatest selectivity (high proton conductivity as well as very low methanol permeability). This could be explained as follows: the protons are transported by the proton hopping which is facilitated by the -SO<sub>3</sub>H groups of the sCMK-3/SPEEK nanocomposite which is distributed within the membrane matrix. These sulfonic acid groups can behave as weak Lewis-base sites which promote the through-plane transport of protons.

The hydrolytic stability of the membranes was determined as their weight loss and surface chemical structure after long term exposure to water. The prepared membranes showed no discernible weight loss or change in chemical structure even after 90 days.

The prepared membranes are compared with the recent state-of-the-art membranes reported by other researchers and are tabulated in Table 3. In general, we observed that membranes with a Nafion backbone displayed a high IEC value and hence good proton conductivity. It is observed that the sCMK-3 prepared by nano-casting followed by sulfonation improves the performance when incorporated as a nanocomposite using SPEEK. The prepared membranes, in particular, M4, holds a good potential to be explored in the fuel-cell test kit to determine the cell efficiency.

## 4 Conclusions

We report a novel nanocomposite- SPEEK/sCMK-3 incorporated into PVDF membranes for testing its potential as a proton exchange membrane. The sulfonation of the mesoporous carbon nanofiller was carried out successfully by a facile one-step method and confirmed by various characterization techniques. The chemical analysis and the change in morphology of the membranes confirm the incorporation of the nanocomposite into the membrane matrix. The results of water contact angle, water uptake and swelling ratio indicates an increase in the hydrophilicity of the membranes upon the addition of SPEEK/sCMK-3. The availability of extra sulfonic acid groups enhances the water affinity of the membranes through hydrogen bonding. The sulfonic acid sites are responsible for the greater ion-exchange capacity of the membranes and these form

a water bridge which enhanced the through-plane proton conductivity. These membranes exhibited considerable thermal stability and exceptional hydrolytic stability. It is observed that M4 shows high proton conductivity with sufficiently diminished methanol permeability indicating that the membrane is suitable to be explored as a potential replacement for Nafion in DMFCs.

## Compliance with ethical standards

**Conflict of interest** The authors report no conflict of interest.

## References

- Power Sector in India (n.d.) Market Size, Industry Analysis, Govt Initiatives | IBEF (Govt. Trust). <https://www.ibef.org/industry/power-sector-india.aspx>. Accessed 2 March 2020
- Uma Devi A, Muthumeenal A, Sabarathinam RM, Nagendran A (2017) Fabrication and electrochemical properties of SPVdF-co-HFP/SPES blend proton exchange membranes for direct methanol fuel cells. *Renew Energy* 102:258–265. <https://doi.org/10.1016/j.renene.2016.10.060>
- Apak S, Atay E, Tuncer G (2017) Renewable hydrogen energy and energy efficiency in Turkey in the 21st century. *Int J Hydrog Energy* 42:2446–2452. <https://doi.org/10.1016/j.ijhydene.2016.05.043>
- Li X, Faghri A (2013) Review and advances of direct methanol fuel cells (DMFCs) part I: design, fabrication, and testing with high concentration methanol solutions. *J Power Sources* 226:223–240. <https://doi.org/10.1016/j.jpowsour.2012.10.061>
- Aricò A, Sebastian D, Schuster M, Bauer B, D'Urso C, Lufrano F, Baglio V, Aricò AS, Sebastian D, Schuster M, Bauer B, D'Urso C, Lufrano F, Baglio V (2015) Selectivity of direct methanol fuel cell membranes. *Membranes (Basel)* 5:793–809. <https://doi.org/10.3390/membranes5040793>
- Roy A, Hickner MA, Lee H-S, Glass T, Paul M, Badami A, Riffle JS, McGrath JE (2017) States of water in proton exchange membranes: part A—influence of chemical structure and composition. *Polymer (Guildf)* 111:297–306. <https://doi.org/10.1016/j.polymer.2017.01.021>
- Mondal S, Soam S, Kundu PP (2015) Reduction of methanol crossover and improved electrical efficiency in direct methanol fuel cell by the formation of a thin layer on Nafion 117 membrane: Effect of dip-coating of a blend of sulphonated PVdF-co-HFP and PBI. *J Membr Sci* 474:140–147. <https://doi.org/10.1016/j.memsci.2014.09.023>
- Chien H-C, Tsai L-D, Huang C-P, Kang C, Lin J-N, Chang F-C (2013) Sulfonated graphene oxide/Nafion composite membranes for high-performance direct methanol fuel cells. *Int J Hydrog Energy* 38:13792–13801. <https://doi.org/10.1016/j.ijhydene.2013.08.036>
- Yan XH, Wu R, Xu JB, Luo Z, Zhao TS (2016) A monolayer graphene—Nafion sandwich membrane for direct methanol fuel cells. *J Power Sources* 311:188–194. <https://doi.org/10.1016/j.jpowsour.2016.02.030>
- Guo Z, Xu X, Xiang Y, Lu S, Jiang SP (2015) New anhydrous proton exchange membranes for high-temperature fuel cells based on PVDF–PVP blended polymers. *J Mater Chem A* 3:148–155. <https://doi.org/10.1039/C4TA04952G>
- Wang J, Gong C, Wen S, Liu H, Qin C, Xiong C, Dong L (2018) Proton exchange membrane based on chitosan and solvent-free carbon nanotube fluids for fuel cells applications. *Carbohydr Polym* 186:200–207. <https://doi.org/10.1016/j.carbpol.2018.01.032>
- Neelakandan S, Muthumeenal A, Rana D, Kaleekkal NJ, Nagendran A (2019) Sulfonated poly(phenylene ether ether sulfone) membrane tailored with layer-by-layer self-assembly of poly(diallyldimethylammonium chloride) and phosphotungstic acid for DMFC applications. *J Appl Polym Sci* 136:47344. <https://doi.org/10.1002/app.47344>
- Kim AR, Vinothkannan M, Yoo DJ (2017) Sulfonated-fluorinated copolymer blending membranes containing SPEEK for use as the electrolyte in polymer electrolyte fuel cells (PEFC). *Int J Hydrog Energy* 42:4349–4365. <https://doi.org/10.1016/j.ijhydene.2016.11.161>
- Gong X, He G, Wu Y, Zhang S, Chen B, Dai Y, Wu X (2017) Aligned electrospun nanofibers as proton conductive channels through thickness of sulfonated poly(phthalazinone ether sulfone ketone) proton exchange membranes. *J Power Sources* 358:134–141. <https://doi.org/10.1016/j.jpowsour.2017.05.022>
- Rambabu G, Bhat SD (2014) Simultaneous tuning of methanol crossover and ionic conductivity of sPEEK membrane electrolyte by incorporation of PSSA functionalized MWCNTs: a comparative study in DMFCs. *Chem Eng J* 243:517–525. <https://doi.org/10.1016/j.cej.2014.01.030>
- Arias JJR, Carlos Dutra J, de S Gomes A (2017) Hybrid membranes of sulfonated poly ether ether ketone, ionic liquid and organically modified montmorillonite for proton exchange membranes with enhanced ionic conductivity and ionic liquid leach protection. *J Membr Sci* 537:353–361. <https://doi.org/10.1016/j.memsci.2017.05.044>
- He D, Tang H, Kou Z, Pan M, Sun X, Zhang J, Mu S (2017) Engineered graphene materials: synthesis and applications for polymer electrolyte membrane fuel cells. *Adv Mater* 29:1601741. <https://doi.org/10.1002/adma.201601741>
- Abdullah N, Kamarudin SK (2015) Titanium dioxide in fuel cell technology: an overview. *J Power Sources* 278:109–118. <https://doi.org/10.1016/j.jpowsour.2014.12.014>
- Simari C, Lo Vecchio C, Enotiadis A, Davoli M, Baglio V, Nicotera I (2019) Toward optimization of a robust low-cost sulfonated-polyethersulfone containing layered double hydroxide for PEM fuel cells. *J Appl Polym Sci*. <https://doi.org/10.1002/app.47884>
- Zhen D, He G, Xu X, Yan X, Du N, Gong X, Li T, Dai Y, Wu X (2018) Simultaneous enhancement of proton conductivity and methanol resistance of sulfonated poly(phthalazinone ether sulfone ketone)/superacid sulfated zirconia composite membranes for direct methanol fuel cells. *J Appl Polym Sci* 135:46758. <https://doi.org/10.1002/app.46758>
- Deng R, Han W, Yeung KL (2018) Confined PFSA/MOF composite membranes in fuel cells for promoted water management and performance. *Catal Today*. <https://doi.org/10.1016/j.cattod.2018.05.016>
- Miculescu M, Thakur VK, Miculescu F, Voicu SI (2016) Graphene-based polymer nanocomposite membranes: a review. *Polym Adv Technol* 27:844–859. <https://doi.org/10.1002/pat.3751>
- Kausar A (2019) Applications of polymer/graphene nanocomposite membranes: a review. *Mater Res Innov* 23:276–287. <https://doi.org/10.1080/14328917.2018.1456636>
- Li C, Wang L, Wang X, Kong M, Zhang Q, Li G (2017) Synthesis of PVDF-g-PSSA proton exchange membrane by ozone-induced graft copolymerization and its application in microbial fuel cells. *J Membr Sci* 527:35–42. <https://doi.org/10.1016/j.memsci.2016.12.065>

25. You PY, Kamarudin SK (2017) Recent progress of carbonaceous materials in fuel cell applications: an overview. *Chem Eng J* 309:489–502. <https://doi.org/10.1016/J.CEJ.2016.10.051>
26. Kaleekkal NJ, Radhakrishnan R, Sunil V, Kamalanathan G, Sengupta A, Wickramasinghe R (2018) Performance evaluation of novel nanostructured modified mesoporous silica/polyetherimide composite membranes for the treatment of oil/water emulsion. *Sep Purif Technol* 205:32–47. <https://doi.org/10.1016/J.SEPPUR.2018.05.007>
27. Radhakrishnan R, Thiripuranthagan S, Devarajan A, Kumaravel S, Erusappan E, Kannan K (2017) Oxidative esterification of furfural by Au nanoparticles supported CMK-3 mesoporous catalysts. *Appl Catal A Gen* 545:33–43. <https://doi.org/10.1016/J.APCAT.2017.07.031>
28. Xing P, Robertson GP, Guiver MD, Mikhailenko SD, Wang K, Kaliaguine S (2004) Synthesis and characterization of sulfonated poly(ether ether ketone) for proton exchange membranes. *J Membr Sci* 229:95–106. <https://doi.org/10.1016/J.MEMSCI.2003.09.019>
29. Zhang Z-B, Yu X-F, Cao X-H, Hua R, Li M, Liu Y-H (2014) Adsorption of U(VI) from aqueous solution by sulfonated ordered mesoporous carbon. *J Radioanal Nucl Chem* 301:821–830. <https://doi.org/10.1007/s10967-014-3237-4>
30. Al-Othman A, Zhu Y, Tawalbeh M, Tremblay AY, Ternan M (2017) Proton conductivity and morphology of new composite membranes based on zirconium phosphates, phosphotungstic acid, and silicic acid for direct hydrocarbon fuel cells applications. *J Porous Mater* 24:721–729. <https://doi.org/10.1007/s10934-016-0309-6>
31. Gnana Kumar G, Manthiram A (2017) Sulfonated polyether ether ketone/strontium zirconite@TiO<sub>2</sub> nanocomposite membranes for direct methanol fuel cells. *J Mater Chem A* 5:20497–20504. <https://doi.org/10.1039/c7ta06258c>
32. Wang M, Liu G, Tian Z, Shao Y, Wang L, Ye F, Tran MX, Yun Y, Lee JK (2017) Microstructure-modified proton exchange membranes for high-performance direct methanol fuel cells. *Energy Convers Manag* 148:753–758. <https://doi.org/10.1016/J.ENCONMAN.2017.06.020>
33. Zhou X, Wan L-J, Guo Y-G (2012) Facile synthesis of MoS<sub>2</sub>@CMK-3 nanocomposite as an improved anode material for lithium-ion batteries. *Nanoscale* 4:5868. <https://doi.org/10.1039/c2nr31822a>
34. Peng L, Philippaerts A, Ke X, Van Noyen J, De Clippel F, Van Tendeloo G, Jacobs PA, Sels BF (2010) Preparation of sulfonated ordered mesoporous carbon and its use for the esterification of fatty acids. *Catal Today* 150:140–146. <https://doi.org/10.1016/J.CATTOD.2009.07.066>
35. Xia K, Gao Q, Wu C, Song S, Ruan M (2007) Activation, characterization and hydrogen storage properties of the mesoporous carbon CMK-3. *Carbon* 45:1989–1996. <https://doi.org/10.1016/J.CARBON.2007.06.002>
36. Ni D, Sun W, Xie L, Fan Q, Wang Z, Sun K (2018) Bismuth oxyfluoride @ CMK-3 nanocomposite as cathode for lithium ion batteries. *J Power Sources* 374:166–174. <https://doi.org/10.1016/J.JPOWSOUR.2017.11.017>
37. Zheng C, Liu M, Chen W, Zeng L, Wei M (2016) An in situ formed Se/CMK-3 composite for rechargeable lithium-ion batteries with long-term cycling performance. *J Mater Chem A* 4:13646–13651. <https://doi.org/10.1039/C6TA05029H>
38. King AAK, Davies BR, Noorbehesht N, Newman P, Church TL, Harris AT, Razal JM, Minett AI (2016) A new Raman metric for the characterisation of graphene oxide and its derivatives. *Sci Rep* 6:19491. <https://doi.org/10.1038/srep19491>
39. Lu X, Peng Y, Qiu H, Liu X, Ge L (2017) Anti-fouling membranes by manipulating surface wettability and their anti-fouling mechanism. *Desalination* 413:127–135. <https://doi.org/10.1016/J.DESAL.2017.02.022>
40. AG Al Lafi (2014) FTIR spectroscopic analysis of ion irradiated poly (ether ether ketone). *Polym Degrad Stab* 105:122–133. <https://doi.org/10.1016/j.polymdegradstab.2014.04.005>
41. Li X, Zhao Y, Feng Z, Xiang X, Wang S, Xie X, Ramani VK (2017) Ring-opening metathesis polymerization for the preparation of polynorbornene-based proton exchange membranes with high proton conductivity. *J Membr Sci* 528:55–63. <https://doi.org/10.1016/J.MEMSCI.2016.12.050>
42. Hossain MM, Hou J, Wu L, Ge Q, Liang X, Mondal AN, Xu T (2018) Anion exchange membranes with clusters of alkyl ammonium group for mitigating water swelling but not ionic conductivity. *J Membr Sci* 550:101–109. <https://doi.org/10.1016/J.MEMSCI.2017.12.062>
43. Divya K, Sri Abirami Saraswathi MS, Rana D, Alwarappan S, Nagendran A (2018) Custom-made sulfonated poly (ether sulfone) nanocomposite proton exchange membranes using exfoliated molybdenum disulfide nanosheets for DMFC applications. *Polymer (Guildf)* 147:48–55. <https://doi.org/10.1016/j.polymer.2018.05.054>
44. Ayyaru S, Ahn Y-H (2017) Application of sulfonic acid group functionalized graphene oxide to improve hydrophilicity, permeability, and antifouling of PVDF nanocomposite ultrafiltration membranes. *J Membr Sci* 525:210–219. <https://doi.org/10.1016/J.MEMSCI.2016.10.048>
45. Chi B, Hou S, Liu G, Deng Y, Zeng J, Song H, Liao S, Ren J (2018) Tuning hydrophobic-hydrophilic balance of cathode catalyst layer to improve cell performance of proton exchange membrane fuel cell (PEMFC) by mixing polytetrafluoroethylene (PTFE). *Electrochim Acta* 277:110–115. <https://doi.org/10.1016/J.ELECTACTA.2018.04.213>
46. Thakur VK, Lin M-F, Tan EJ, Lee PS (2012) Green aqueous modification of fluoropolymers for energy storage applications. *J Mater Chem* 22:5951. <https://doi.org/10.1039/c2jm15665b>
47. Li J, Zhang Y, Zhang S, Huang X (2015) Sulfonated polyimide/s-MoS<sub>2</sub> composite membrane with high proton selectivity and good stability for vanadium redox flow battery. *J Membr Sci* 490:179–189. <https://doi.org/10.1016/J.MEMSCI.2015.04.053>
48. Liu X, Yang Z, Zhang Y, Li C, Dong J, Liu Y, Cheng H (2017) Electrospun multifunctional sulfonated carbon nanofibers for design and fabrication of SPEEK composite proton exchange membranes for direct methanol fuel cell application. *Int J Hydrog Energy* 42:10275–10284. <https://doi.org/10.1016/J.IJHYDENE.2017.02.128>
49. Pandey RP, Thakur AK, Shahi VK (2014) Sulfonated polyimide/acid-functionalized graphene oxide composite polymer electrolyte membranes with improved proton conductivity and water-retention properties. *ACS Appl Mater Interfaces* 6:16993–17002. <https://doi.org/10.1021/am504597a>
50. Cho K-Y, Eom J-Y, Jung H-Y, Choi N-S, Lee YM, Park J-K, Choi J-H, Park K-W, Sung Y-E (2004) Characteristics of PVdF copolymer/Nafion blend membrane for direct methanol fuel cell (DMFC). *Electrochim Acta* 50:583–588. <https://doi.org/10.1016/J.ELECTACTA.2004.03.063>
51. Krathumkhet N, Vongjitpimol K, Chuesutham T, Changkhamchom S, Phasuksom K, Sirivat A, Wattanakul K (2018) Preparation of sulfonated zeolite ZSM-5/sulfonated polysulfone composite membranes as PEM for direct methanol fuel cell application. *Solid State Ionics* 319:278–284. <https://doi.org/10.1016/J.SSI.2018.02.019>
52. Sahoo M, Perez-page M, Kalangi V, Nair RR, Holmes S (2018) Monolayer graphene based membrane to replace Nafion in PEM fuel cells. *Meet. Abstr. MA2018-01* 1763–1763
53. Liu D, Peng J, Li Z, Liu B, Wang L (2018) Improvement in the mechanical properties, proton conductivity, and methanol

- resistance of highly branched sulfonated poly(arylene ether)/graphene oxide grafted with flexible alkylsulfonated side chains nanocomposite membranes. *J Power Sources* 378:451–459. <https://doi.org/10.1016/J.JPOWSOUR.2017.12.057>
54. Parthiban V, Akula S, Peera SG, Islam N, Sahu AK (2016) Proton conducting Nafion-sulfonated graphene hybrid membranes for direct methanol fuel cells with reduced methanol crossover. *Energy Fuels* 30:725–734. <https://doi.org/10.1021/acs.energyfuels.5b02194>
  55. Dutta K, Das S, Kumar P, Kundu PP (2014) Polymer electrolyte membrane with high selectivity ratio for direct methanol fuel cells: a preliminary study based on blends of partially sulfonated polymers polyaniline and PVdF-co-HFP. *Appl Energy* 118:183–191. <https://doi.org/10.1016/J.APENERGY.2013.12.029>
  56. Yang T (2009) Composite membrane of sulfonated poly(ether ether ketone) and sulfated poly(vinyl alcohol) for use in direct methanol fuel cells. *J Membr Sci* 342:221–226. <https://doi.org/10.1016/J.MEMSCI.2009.06.045>
  57. Bagheri A, Javanbakht M, Hosseinabadi P, Beydaghi H, Shabanikia A (2018) Preparation and characterization of SPEEK/SPVDF-co-HFP/LaCrO<sub>3</sub> nanocomposite blend membranes for direct methanol fuel cells. *Polymer (Guildf)* 138:275–287. <https://doi.org/10.1016/J.POLYMER.2018.01.049>
  58. Jiang Z-J, Jiang Z, Tian X, Luo L, Liu M (2017) Sulfonated holey graphene oxide (SHGO) filled sulfonated poly(ether ether ketone) membrane: the role of holes in the SHGO in improving its performance as proton exchange membrane for direct methanol fuel cells. *ACS Appl Mater Interfaces* 9:20046–20056. <https://doi.org/10.1021/acsami.7b00198>
  59. Parthiban V, Akula S, Sahu AK (2017) Surfactant templated nanoporous carbon-Nafion hybrid membranes for direct methanol fuel cells with reduced methanol crossover. *J Membr Sci* 541:127–136. <https://doi.org/10.1016/J.MEMSCI.2017.06.081>
  60. Cheng T, Feng M, Huang Y, Liu X (2017) SGO/SPEN-based highly selective polymer electrolyte membranes for direct methanol fuel cells. *Ionics (Kiel)* 23:2143–2152. <https://doi.org/10.1007/s11581-017-2057-2>
  61. Wang B, Hong L, Li Y, Zhao L, Zhao C, Na H (2017) Property enhancement effects of side-chain-type naphthalene-based sulfonated poly(arylene ether ketone) on Nafion composite membranes for direct methanol fuel cells. *ACS Appl Mater Interfaces* 9:32227–32236. <https://doi.org/10.1021/acsami.7b08566>
  62. Molla-Abbasi P, Janghorban K, Asgari MS (2018) A novel heteropolyacid-doped carbon nanotubes/Nafion nanocomposite membrane for high performance proton-exchange methanol fuel cell applications. *Iran Polym J* 27:77–86. <https://doi.org/10.1007/s13726-017-0587-0>
  63. Prakash O, Jana KK, Jain R, Shah P, Manohar M, Shahi VK, Maiti P (2018) Functionalized poly(vinylidene fluoride-co-hexafluoro propylene) membrane for fuel cell. *Polymer (Guildf)* 151:261–268. <https://doi.org/10.1016/J.POLYMER.2018.07.086>
  64. Amoozadeh A, Mazdarani H, Beydaghi H, Tabrizian E, Javanbakht M (2018) Novel nanocomposite membrane based on Fe<sub>3</sub>O<sub>4</sub>@TDI@TiO<sub>2</sub>-SO<sub>3</sub>H: hydration, mechanical and DMFC study. *New J Chem* 42:16855–16862. <https://doi.org/10.1039/C8NJ03646B>
  65. Liu X, Zhang Y, Chen Y, Li C, Dong J, Zhang Q, Wang J, Yang Z, Cheng H (2017) A superhydrophobic bromomethylated poly(phenylene oxide) as a multifunctional polymer filler in SPEEK membrane towards neat methanol operation of direct methanol fuel cells. *J Membr Sci* 544:58–67. <https://doi.org/10.1016/J.MEMSCI.2017.09.013>

**Publisher's Note** Springer Nature remains neutral with regard to jurisdictional claims in published maps and institutional affiliations.